Technical
Note: M41010

Rotational and Tidal Agitation Fluid Exchange in Comparison of Tissue Processors

Conducted by: Western Michigan University (WMU) Fluids Laboratory
Research Period: September 1, 2005 to December 30, 2005
Authored By: Dr. Parviz Merati, Jared Boyd, Hueng Leong
For: Richard-Allan Scientific, a subsidiary of Thermo Fisher Scientific
4481 Campus Drive, Kalamazoo, MI 49008, USA

Abstract

Tissue processors currently in use in histology laboratories today are designed to facilitate the replacement of water-based fixatives through a series of dehydration, clearing and infiltration steps culminating in a paraffin-infiltrated tissue sample. The process of exchanging the various fluids is based on tissue sample immersion combined with gentle agitation. In all traditional tissue processors this process is time consuming, frequently taking up to 10 or more hours to complete a cycle. As a result, the tissue processing step is often the greatest workflow bottleneck within the histology laboratory.

Efforts to speed up tissue processing have resulted in instrument designs that include higher processing temperatures and/or the use of microwaves at one or more points during tissue processing. However, higher temperatures and microwaves can adversely affect tissue morphology subsequently leading to artifacts and poor quality primary or specialty staining. In addition, constraints on tissue thickness and tissue type to accommodate higher temperatures or microwaves have made these designs useful for only certain applications limiting their contribution towards reducing overall tissue processing times.

The current study introduces a new design in tissue processors termed rotational agitation and compares it with traditional processors utilizing simple immersion and agitation techniques frequently termed tidal agitation. Rotational agitation performed at conventional processing temperatures and without the use of microwaves offers the advantages of traditional processing in a fraction of the time. A series of measurements designed to compare the two methods clearly show the advantages of rotational agitation by providing an overall seven-fold improvement in fluid exchange efficiency.

Introduction

The purpose of this investigation is to determine and compare the flow fields within the tissue processing cassettes of two different tissue processing machines. Previous investigation was conducted on a tidal agitation tissue processor to determine the flow fields within two different cassettes within the same machine, and determine which was superior. Although the goal of the previous investigation was to compare flow fields within two different cassette designs, insight into the flow fields within the cassettes for this machine as a whole was obtained.

The majority of tissue processors utilize tidal flooding with a mechanical stirrer below the cassettes to induce interaction between the fixative fluids and the tissue samples. The new Thermo Scientific rotational tissue processor (RTP) utilizes a rotating rack to induce interaction between the fixative fluids and the tissue samples. Hereafter in the report, the traditional tissue processor and the RTP tissue processor will be referred to as the tidal agitation processor and the RTP processor, respectively.

Particle image velocimetry (PIV) and Planar laser-induced fluorescence (PLIF) measurements within the tissue cassettes are taken for both machines to compare and contrast the flow fields within the cassettes of each machine. The results show that the new machine has superior flow within the cassettes. Superior flow is characterized by flow fields with higher volumetric flow rates through the cassettes. Higher flow rates through the cassettes mean that more fluid is passing over the tissue within the cassette during the same time interval, which correlates to faster tissue processing.

In addition, PLIF was used to visualize the flow around the Total Biopsy Cassette II which was re-designed in the first phase of this research. The PLIF pictures show the details of flow motion within the cassette and its behavior as exits through one millimeter diameter holes in the back of the cassettes.

Experimental Setup

Models of both processors were built for the PIV and PLIF measurements. This involved creating processors similar to the actual processors with clear reservoirs to allow PIV and PLIF measurements to be taken. Care was taken to assure geometric similarity between the model processors and the actual processors. Cassette racks and cassettes within each processor were provided by Thermo Fisher Scientific, and were also modified slightly to allow measurements to be taken. These modifications involved removing small portions of the racks and cassettes to provide a clear view of the interior of the cassettes. Also, all cassettes were empty to allow a better comparison between processors, since placement of tissue samples within the cassettes would significantly affect the flow fields.

The tidal agitation processor was replicated by constructing a clear acrylic reservoir, with the stirrer and cassette rack located within it. The tidal agitation processor is designed to have two cassette racks stacked within the reservoir. To obtain PIV and PLIF data for the lower rack, the upper rack had to be removed to allow the laser light to pass through the setup. As such, data for the lower rack is obtained without the presence of the upper rack. The acrylic reservoir with the modified cassette colored in black for single and double rack experiments is shown in Figure 1.

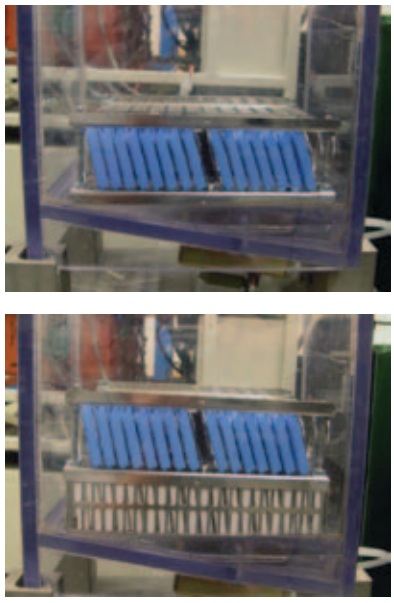

Figure 1.
Tidal Agitation Processor's Acrylic Reservoir

The simulated tidal agitation processor with the PIV and PLIF setup is shown in Figure 2. This figure shows both racks in the processor. Replicating the RTP processor was somewhat more complicated due to its complex geometry shape. The actual processor consists of a bowl shaped reservoir with several rotating cassette racks. Rotation of the cassette racks is accomplished by utilizing a magnetic drive to rotate the cassette racks. Use of this drive system for the model processor would be expensive and problematic. As such, the model processor utilizes a DC motor with reduction gears to rotate a shaft attached to the cartridge racks. The drive system was designed to simulate the 8 rpm rotation of the actual processor. The reservoir bowl for the model processor was constructed of 3/16" thick acrylic plastic using thermoforming technique at WMU's Plastics Laboratory. A foundation for the reservoir was constructed of aluminum. The foundation provides a method of supporting the reservoir, and is designed to support the rotating shaft, mechanical seals and bearings. The simulated RTP processor with PIV and PLIF setup is shown in Figure 3.

PIV and PLIF measurements within the tidal agitaion processor are easily obtained, since the cassettes are stationary relative to the camera. However, the cassettes within the RTP processor pass through the view of the camera. As such, a mechanism was required to allow measurements to be taken with the cassettes located at the same position relative to the camera for each revolution. To accomplish this, a mechanical switch was utilized to trigger the laser and camera each time the cassette rotates into position directly in front of the camera. A stainless steel collar with a detent was manufactured to fit around the rotating shaft, and is held in place on the shaft with a setscrew. This allows the detent on the collar to be positioned at any angle on the shaft. A mechanical switch was then attached to the base of the processor. The mechanical switch is triggered each time the detent on the collar passes. The switch sends a 5 volt TTL signal to the laser synchronizer each time the detent on the collar passes it. The detent on the collar is

Figure 2
Tidal Agitation Processor Setup

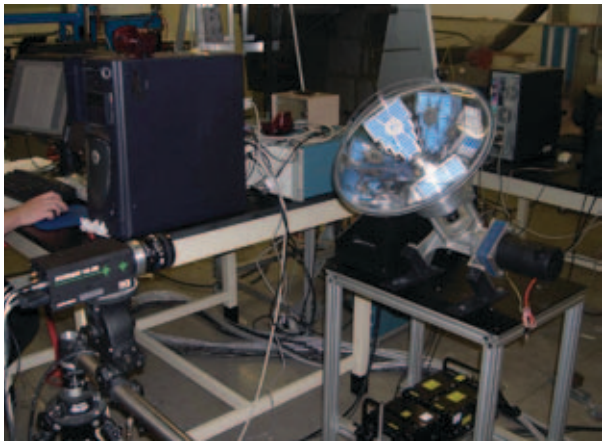

Figure 3
RTP Processor Setup

located angularly on the shaft relative to the cassette of interest such that the synchronizer will trigger each time the cassette passes directly in front of the camera. In this way measurements can be taken with the cassette fixed relative to the camera. The cassettes of interest were painted black to reduce reflection of the laser light, which would have negatively effected data collection. The experimental setup showing a close up of the rotating racks and the cassettes of interest is shown in Figure 4.

Enlarged views of the cassettes within the rack are shown in Figure 5. In this photo the cassettes of interest can be easily seen. The front sides of the cassettes were removed to allow a view into the cassettes, and then covered with a thin piece of transparency film to maintain geometric similarity to the intact cassettes. The transparency film can also be seen in the photo.

There are five rows of cassettes within each rack. A series of data was taken for cassettes located in the outermost three rows. Figure 5 shows the cassettes positioned in the outermost row. Figure 4 shows the cassettes positioned in the second row back from the outermost row. A third set of data was taken for cassettes positioned in the third row back from the outside, which is not shown in any figures. Data was taken for three cassettes in each row, and centered in the rack. These three cassettes as shown in Figure 4 have been glued together with four other intact cassettes (two leading and two trailing) to form a block. This was done to prevent shifting of the cassettes and to allow more accurate positioning within the rack. Care was taken not to obstruct any openings in the cassettes.

PLIF images were taken for both machines, using Rhodium B dye. For the RTP processor, cassettes were submerged in the dye and frozen. The cassettes were then broken apart and excess dye was removed from the outside of the cassette, leaving a frozen portion of dye within the cassette. The cassette was then placed upstream of the cassettes of interest. The dye was then released upon submersion, by natural melting processes. For the tidal agitation processor dye was injected with a standard pipette in close proximity to the cassette of interest.

PIV measurements in both processors are taken using a TSI synchronizer, Insight 5 software, PIV 10-30 camera with filter, and Big Sky lasers. Water with low concentrations of 5μm hollow glass sphere seeding particles was used as the fluid in each processor. Processing of the raw data is done with Insight 5 software, custom LabVIEW program, and TecPlot.

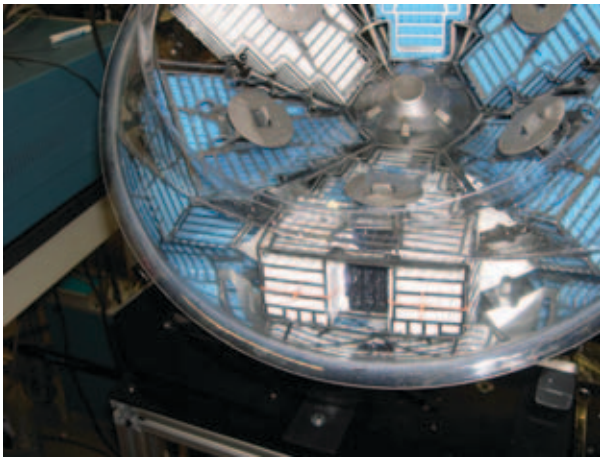

Figure 4
Rack and Cassette in RTP Processor

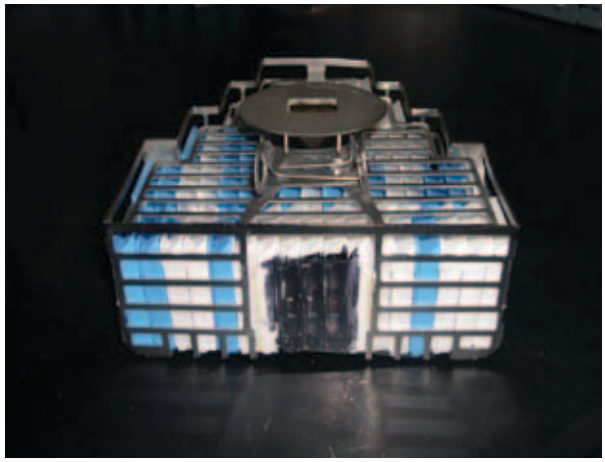

Figure 5
Cassette Rack and Cassettes of Interest

PLIF Results for RTP Processor

PLIF data was only collected for the cassettes located in the outermost row of the cassette racks (row 1). A series of images was taken as the cassettes passed in front of the camera, to allow better visualization of the transient nature of the flow field within the cassettes. Due to the fact that the cassettes only pass in front of the camera for a brief interval, and a longer series of images was desired, the researchers slowed the rotation of the RTP processor to obtain a half speed video. By slowing the rotation of the cassettes, a longer series of images could be obtained. However, the flow fields within the cassettes at this slower speed were significantly different from the full speed images. The PLIF images shown in this report are obtained from the full speed PLIF measurements.

Based on detailed flow visualization studies, generally we have observed two dominant flow structures within the cassettes, one under the conditions where the cassettes are traveling on the right side of the cassette 2 ($\theta = 0.0$) shown in Figure 6 indicated by the $\theta < 0.0$ flow region. The other is for those situations where the cassettes are moving on the left of the cassette 2, indicated by the $\theta > 0.0$ flow region.

Visualized flow for cassette 3 during its first and second passes in front of the camera view is shown in Figures 7 and 8, respectively. These figures show the instantaneous flow fields of the cassette 3 as the rack passes through about 18 degrees viewing angle for both revolutions (± 9 degrees from $\theta = 0.0$). Since the laser pulse frequency for these images is 30 Hz and the rotational speed of the racks is 8 rpm, the angular displacement between each image is 1.6 degrees, corresponding to about 34 milliseconds between two consecutive images. Although flow structures are similar for both passes, the details of the flow for the second pass are more visible. For $\theta < 0.0$ flow region, higher magnitude of mixing occurs due to the presence of large turbulence generating vortices as the cassettes are filling up with liquid. However, in the $\theta > 0.0$ flow region, the large turbulent structures have died down somewhat, and the smoother flow within the cassettes have had a chance to be developed. Small vortices just downstream of the slots appear and begin to grow as θ increases, most visible in the last four photographs of Figure 8.

It can be seen that small vortices shed from the slots in the cassettes, i.e., each slot sheds two vortices, one with positive and the other with negative vorticity, generating 32 vorticies for the 16 slots along the cassette length as observed by the vorticity contours shown in Figure 20 for row 1 cassettes. The upper half of the cassette is shadowed by a protrusion within the cassette, but the small vortices are also present in the upper half of the cassette. Since there are four rows of these slots along the width of the cassette, the amount of mixing is enhanced by the presence of these small vortices. This will be quantified and elaborated upon during discussion of PIV results.

It should be noted that the PIV data were only taken for cassettes directly in front of the camera, which was located to capture images of the cassettes at the center of submersion within the fluid. It was assumed that the flow within the cassettes at this position would be a good indication of the typical flow field within the cassettes. In reality, the cassettes enter and exit the fluid to either side of the camera view, and data was not collected at these locations. As such, the vortices will form and dissipate in these locations, and further research would be required to quantify this phenomena.

For two revolutions, the flow structures within the three cassettes for an approximate viewing angle of 13 degrees are shown in Figures 9, and 10, respectively. The locations of the cassettes relative to the camera viewing area, indicated by the bright region are shown over each image. The above explanation of the flow behavior for cassette 3 applies to all three cassettes as observed by these images

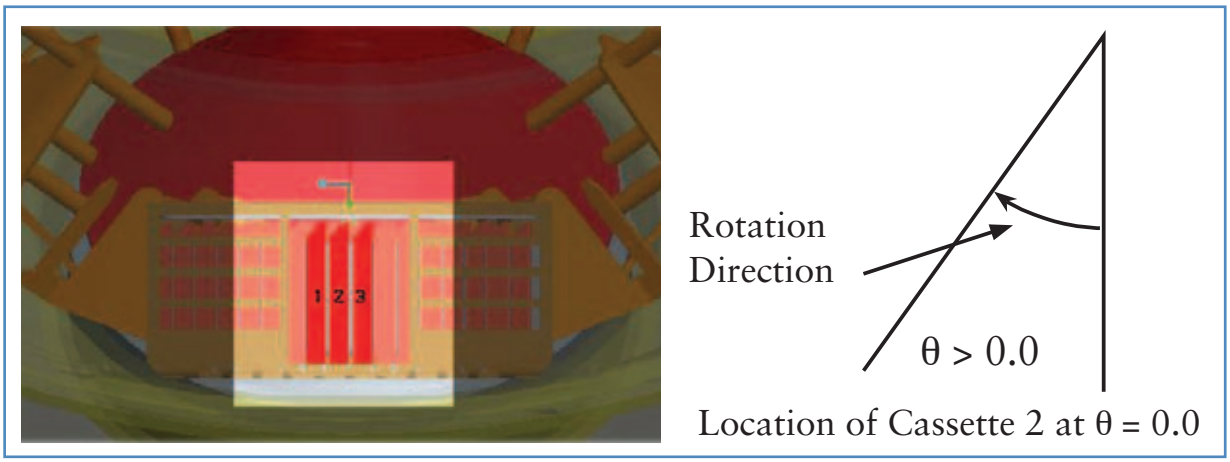

Figure 6

Schematic of the Camera View and the Polar Coordinate System

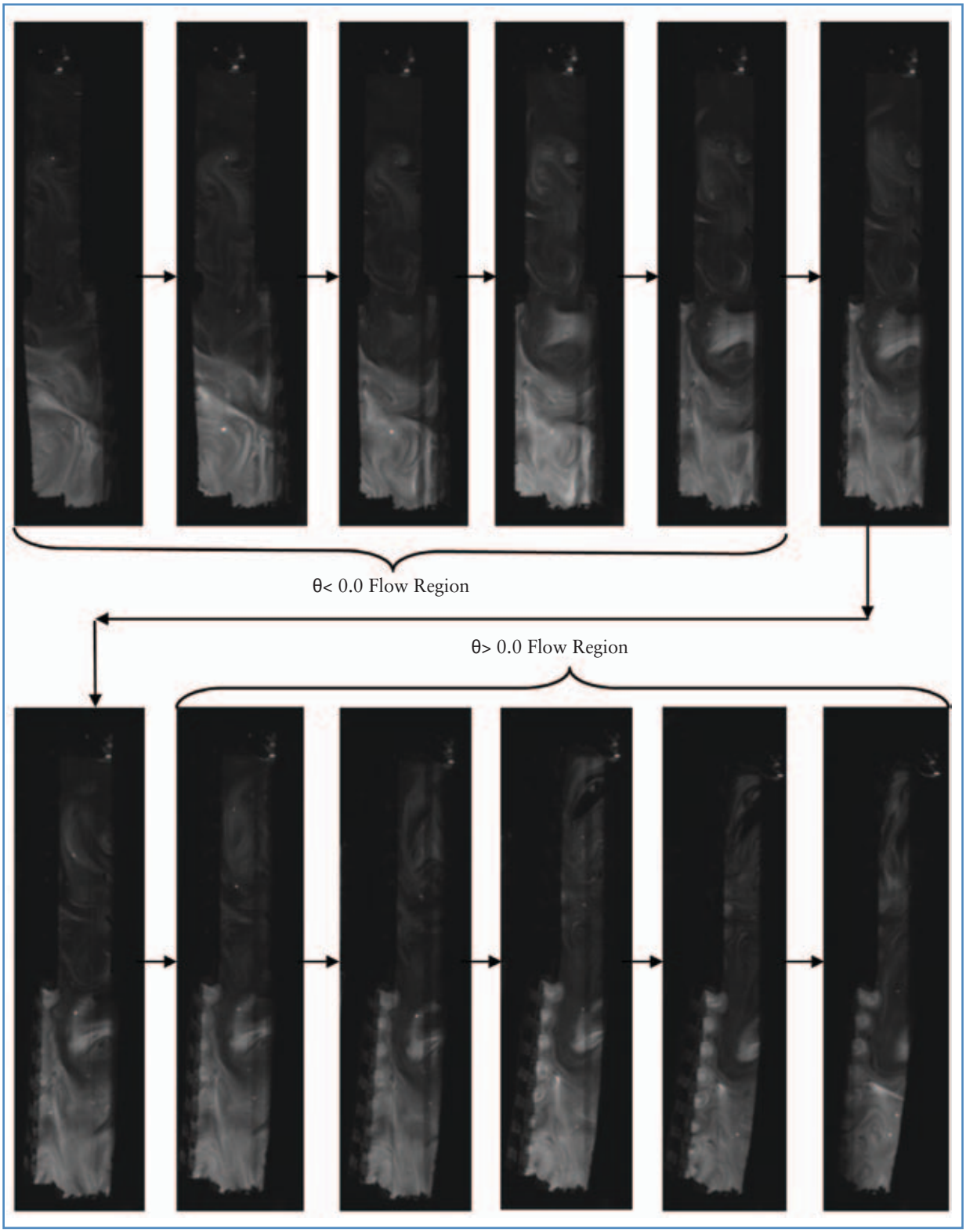

Figure 7

Visualized Flow for Cassette 3 in the First Pass

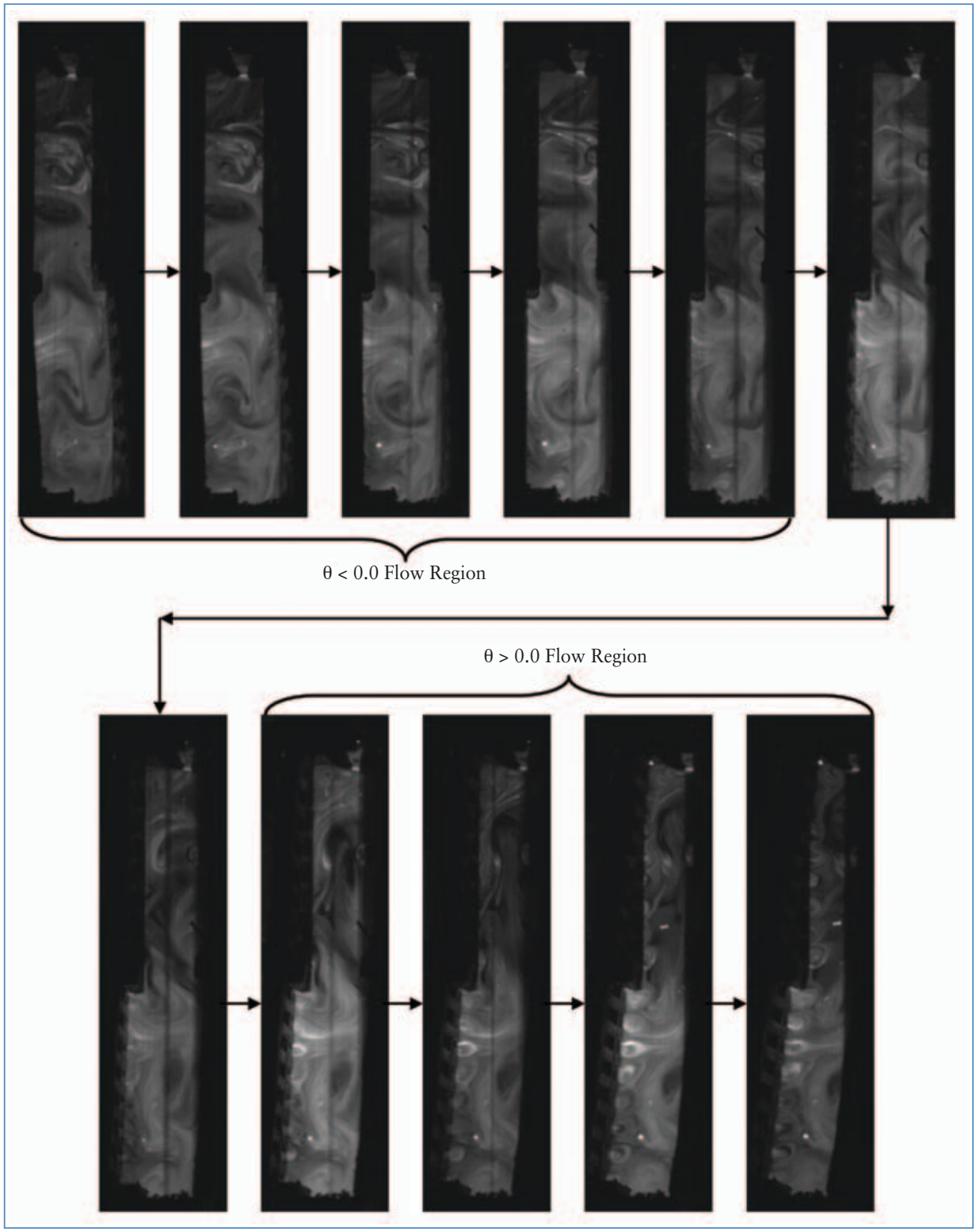

Figure 8

Visualized Flow for Cassette 3 in the Second Pass

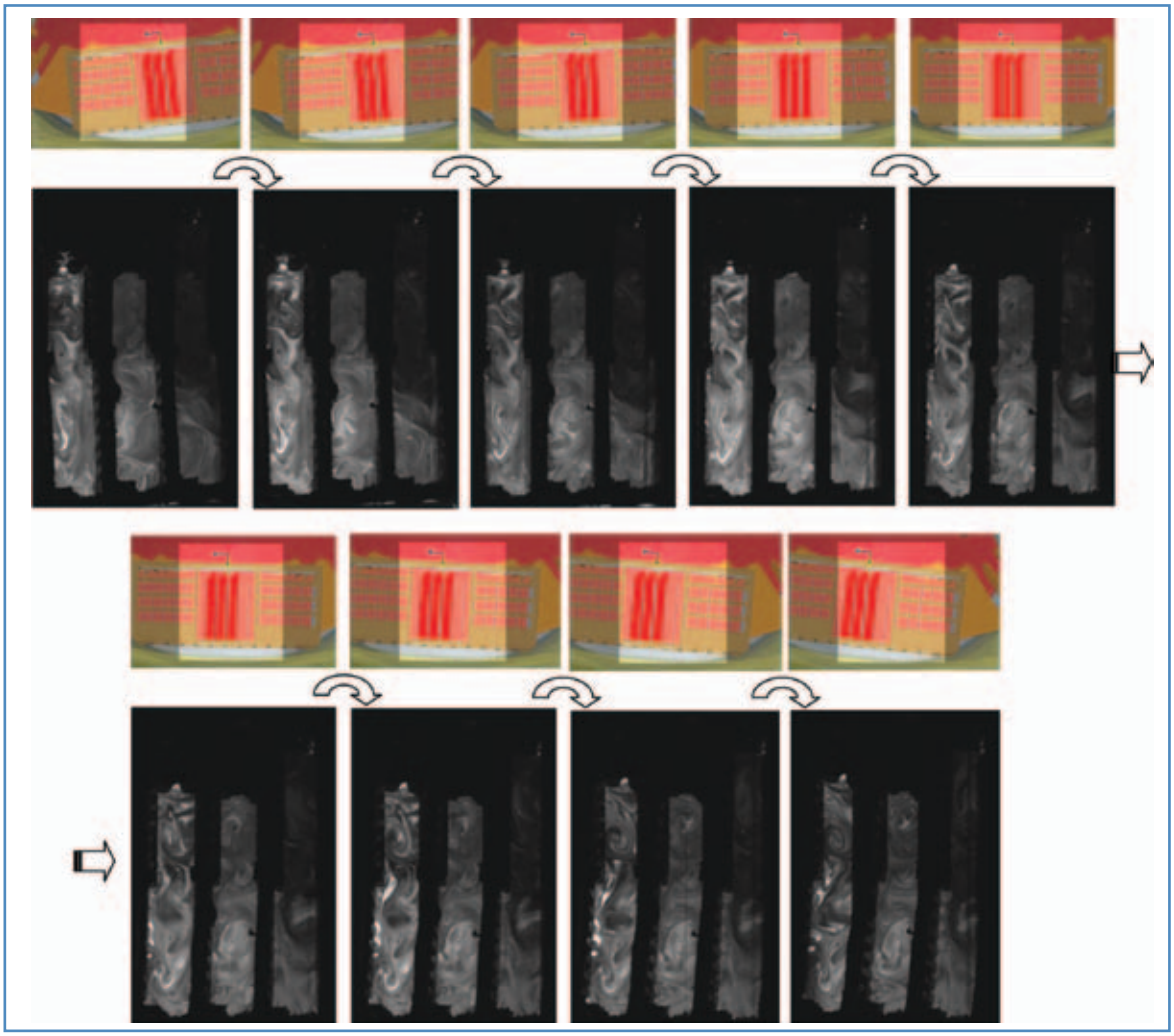

Figure 9

PLIF Pictures for the First Pass

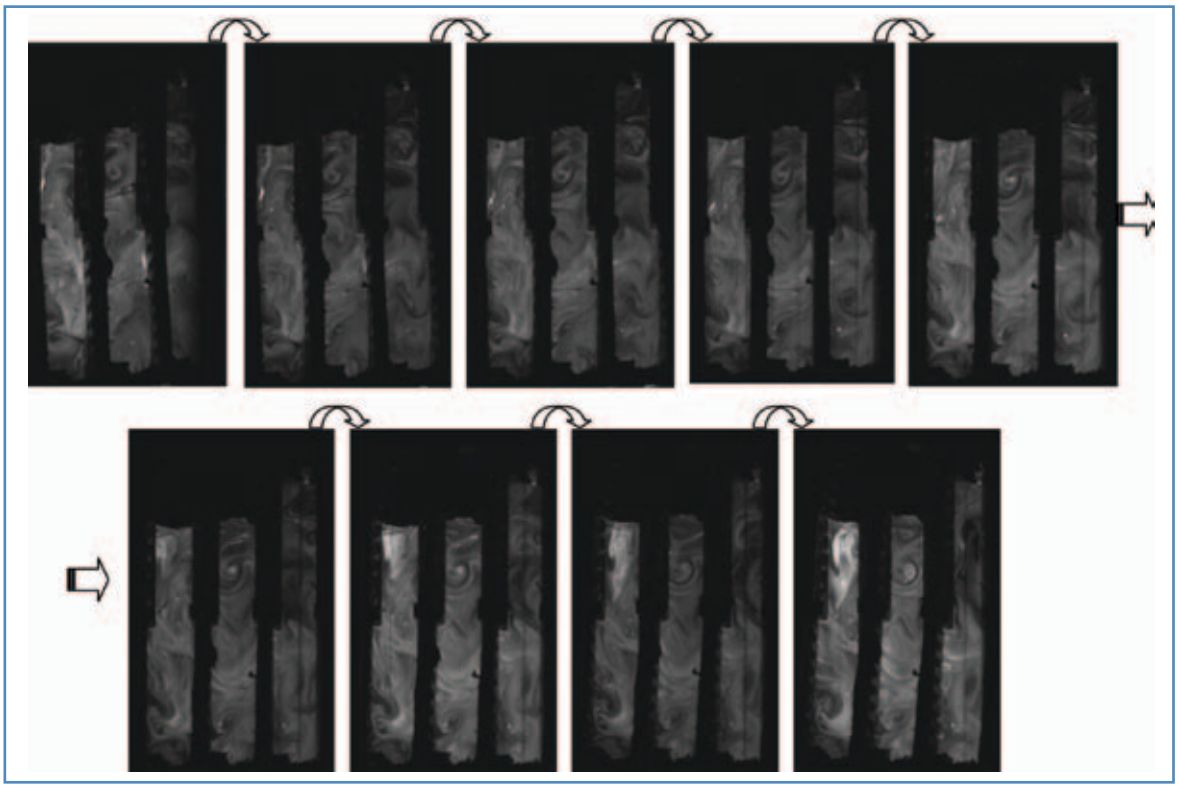

Figure 10

PLIF Pictures for the Second Pass

PIV Results for RTP Processor

PIV data was collected for cassettes located in the three outermost rows of the racks (rows 1,2, and 3, respectively). A series of 20 images was captured for cassettes located in each row, and then averaged to obtain the characteristic flow field at each location. It was observed that bubbles would occasionally form near the top of the cassettes, which yielded bad data for the individual image. As such, images containing bubbles were removed before averaging.

The racks rotate at 8 rpm, which leads to the cassettes having a fixed velocity through the fluid. This fixed rotational velocity is a function of the angular velocity of the racks and the distance from the center of the rotation. As such, the cassettes at the outside of the rack have a higher velocity than the cassettes closer to the axis of rotation. The angular rotational speed of 8 rpm was used with the distance from the center of rotation to the center of the cassette to calculate the fixed velocities of the cassettes. This data is presented in Table 1.

Fixed Velocity Calculations			
rpm = 8.00 rpm ω = 0.1333 rev/s ω = 0.8378 rad/s			
Diameter	**Radius**	**Velocity**	**Velocity**
330	165	138.2301	0.1382
290	145	121.4749	0.1215
250	125	104.7198	0.1047
mm	mm	mm/s	m/s

Table 1

The fluid velocities within the cassettes obtained from PIV measurements are not the true fluid velocities as experienced by the cassette. The true fluid velocities within the cassette are the PIV velocities measured less the fixed velocity of the cassettes. This is due to the fact that the camera is fixed in relation to the RTP processor, and not fixed in relation to the cassette. As such, the fixed velocities were subtracted from the PIV velocities during averaging to obtain the true flow fields within the cassettes.

The velocity flow fields for cassettes in each row are presented in Figures 11-13. These flow fields are the flow fields as seen by the cassettes, and are in line with expectations. Each of these figures shows the flow fields within all three cassettes. The cassettes are moving from right to left in relation to the figures. Figure 11 is data for the outermost row (row 1). Figure 12 is the second row in (row 2). Figure 13 is the third row in (row 3).

The typical velocities within the cassettes are from left to right, which is in line with expectations. As the cassettes move from right to left, fluid is forced through the cassettes. The velocity magnitudes for the two inner rows are similar. However, the velocity magnitude of the fluid in the outermost row seems to be significantly smaller. The researchers believe this is due to fluid being able to escape around the end of the rack, rather than being forced through the rack. The inner rows are surrounded by other cassettes, which do not allow the fluid another avenue of escape, and thus fluid is forced through the cassettes.

The PIV velocity fields were used to create fluid stream traces within the cassettes. These stream traces are shown in Figures 14-16. Once again, data for all three cassettes are shown in each figure. Figure 14 is the outermost row (row 1). Figure 15 is the second row in (row 2). Figure 16 is the third row in (row 3).

The PIV data was also used to create turbulence and vorticity maps within the flow fields. The turbulence data is shown in Figures 17-19. The vorticity data is shown in Figures 20-22. Once again, data for all three cassettes is shown in each figure, and figures are ordered from outermost row to innermost row (row 1 to row 3).

Turbulence intensities within the cassettes are similar between all rows, and seem to be slightly lower in the outer most cassettes. This would be expected since the velocities in the outer row are lower.

The vorticity maps are also similar for all rows. It can be seen that areas of larger vorticity seem to occur in bands, which are aligned with the slots in the cassettes. This would be expected from the PLIF data.

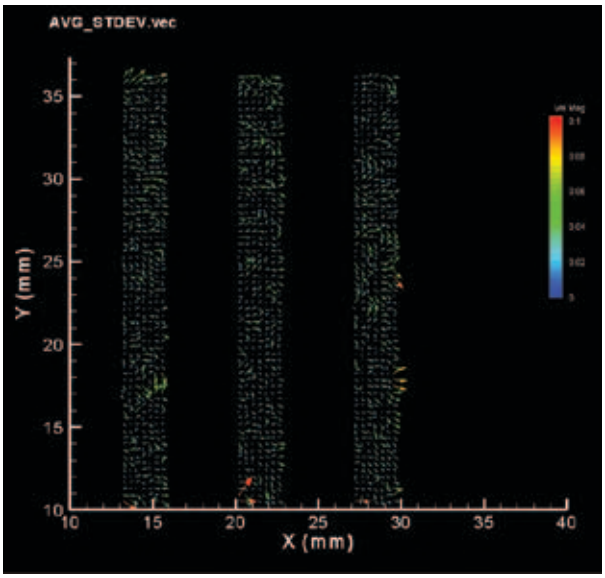

Figure 11

Velocity Flow Field – Row 1

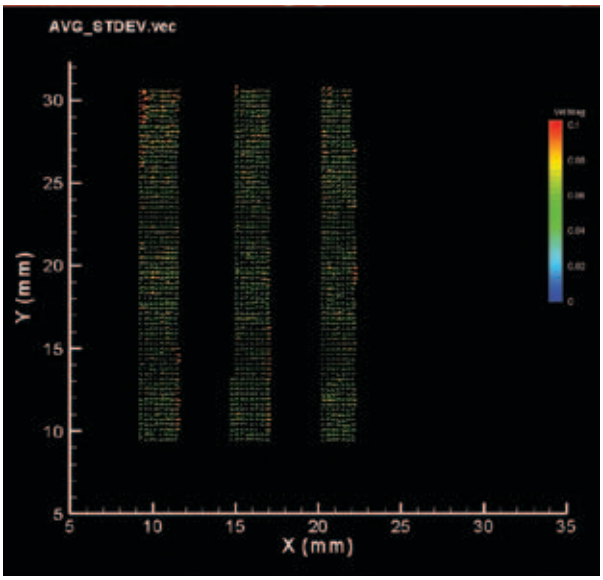

Figure 12

Velocity Flow Field – Row 2

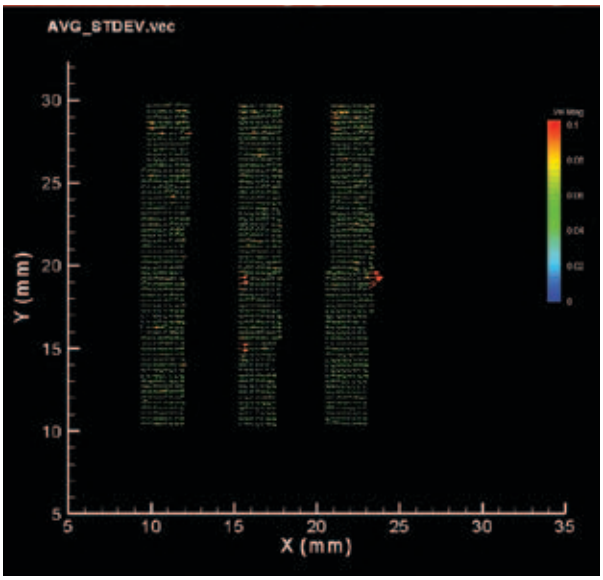

Figure 13

Velocity Flow Field – Row 3

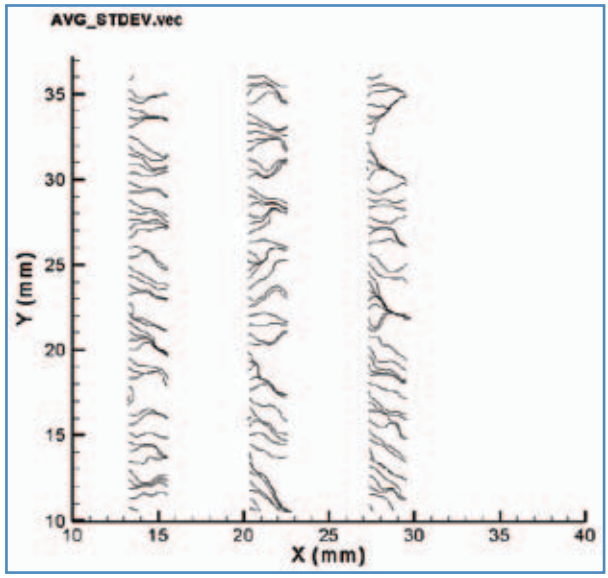

Figure 14

Stream Trace – Row 1

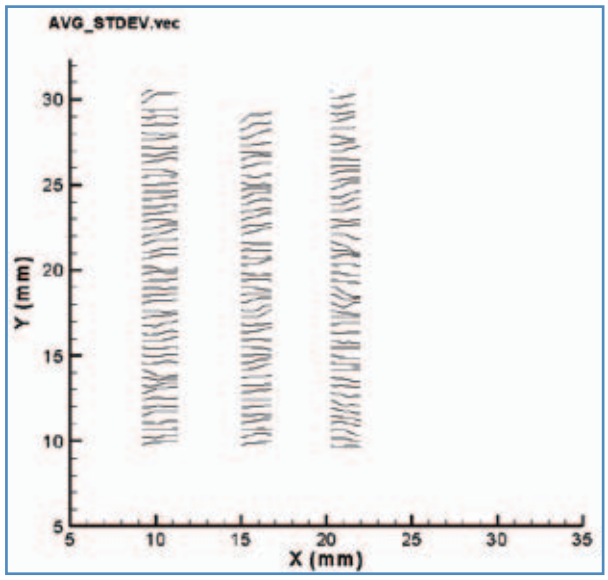

Figure 15

Stream Trace – Row 2

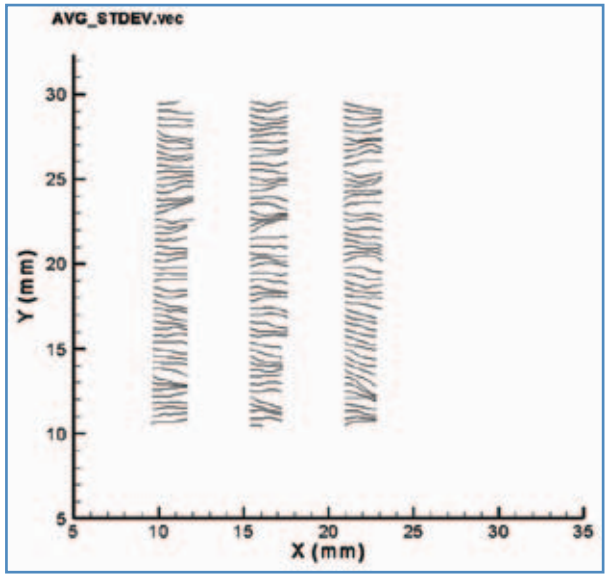

Figure 16

Stream Trace – Row 3

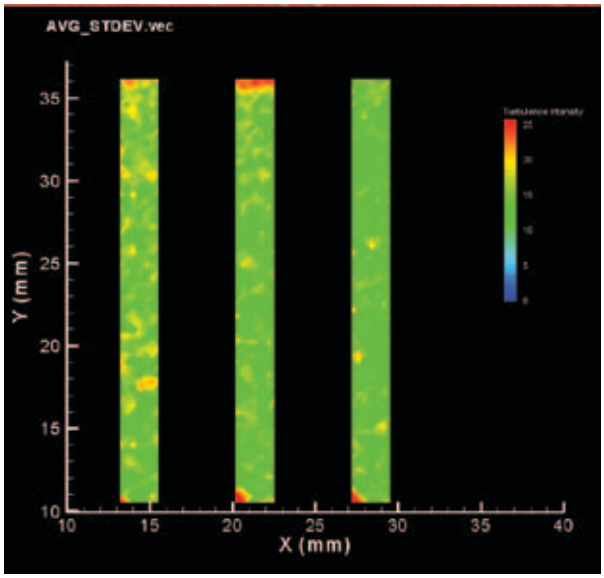

Figure 17

Turbulence Intensity – Row 1

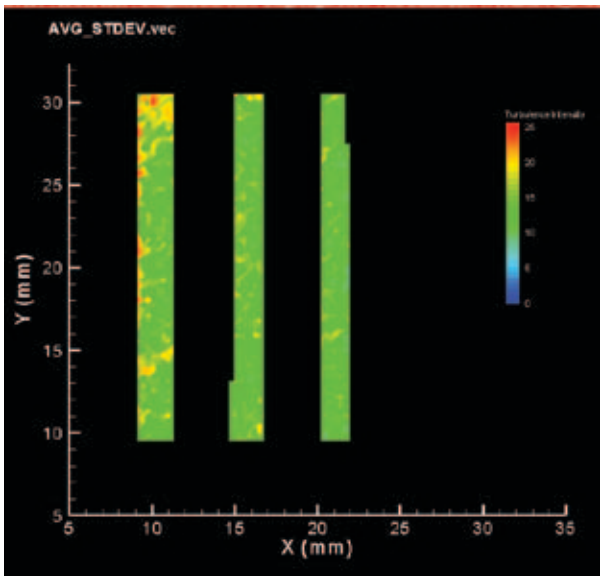

Figure 18

Turbulence Intensity – Row 2

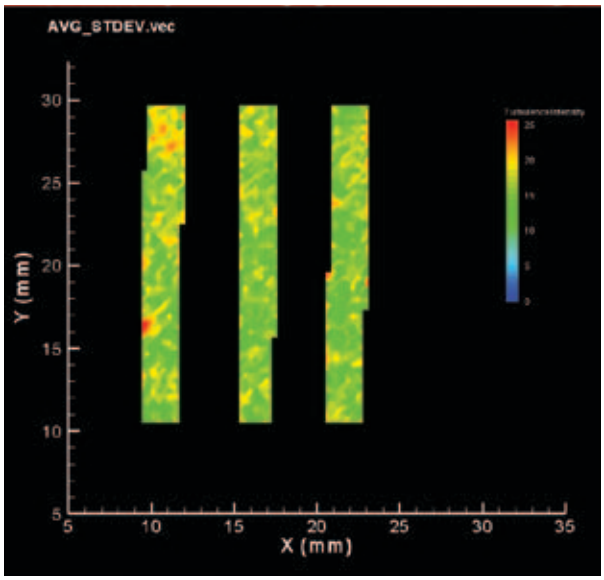

Figure 19

Turbulence Intensity – Row 3

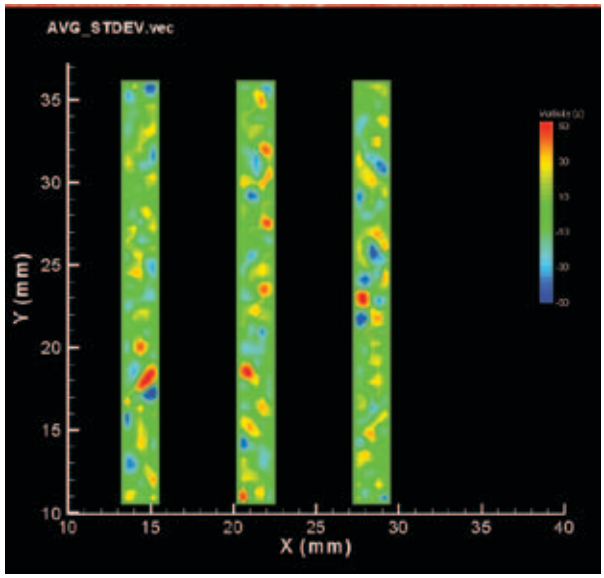

Figure 20

Vorticity – Row 1

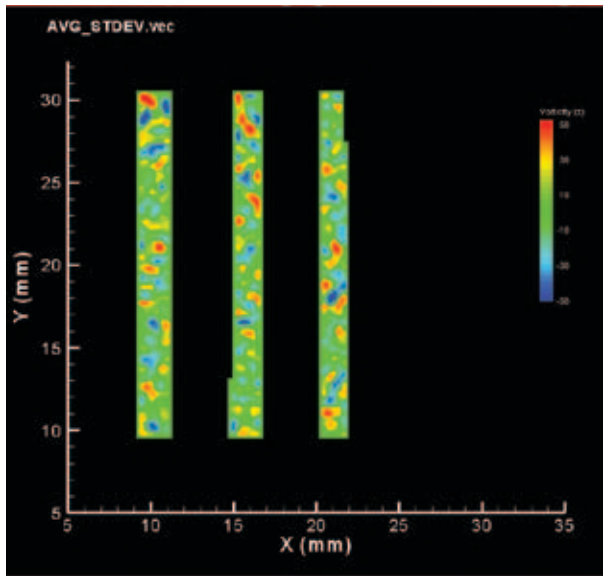

Figure 21

Vorticity – Row 2

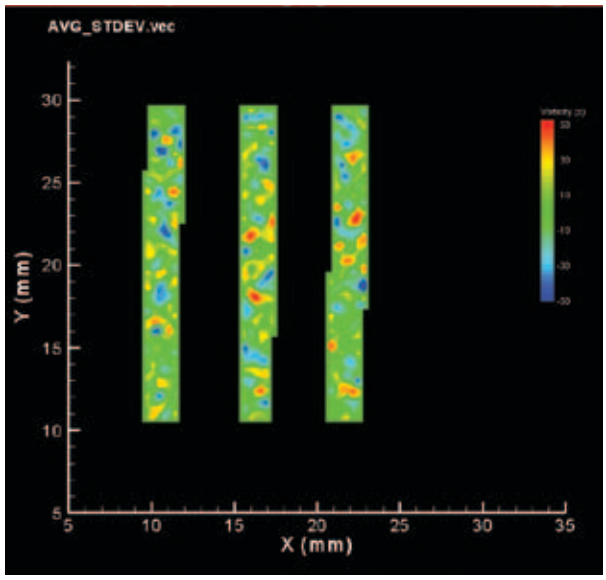

Figure 22

Vorticity – Row 3

PIV Results for RTP Processor Between Racks

Although not of direct interest to the investigation, data was also collected for the flow region between the cassette racks themselves. This was done to obtain insight into the flow field and mixing of the fluid in the areas between the cassette racks. As with the data for cassettes themselves, a velocity field, stream traces, turbulence map, and vorticity map were created for the area between the racks. This data is presented in Figures 23-26.

The fluid seems to travel from left to right above and below the leading rack. It is then entrained behind the leading rack. The turbulence and vorticity maps would seem to indicate that a good deal of mixing is occurring between the racks.

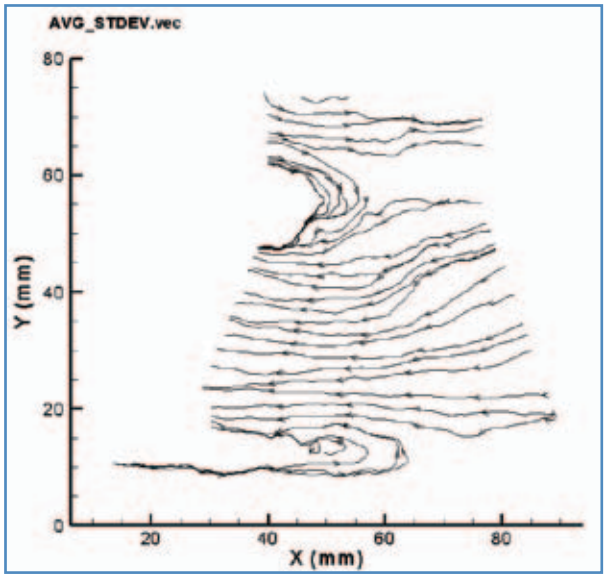

Figure 24

Stream Trace Between Racks

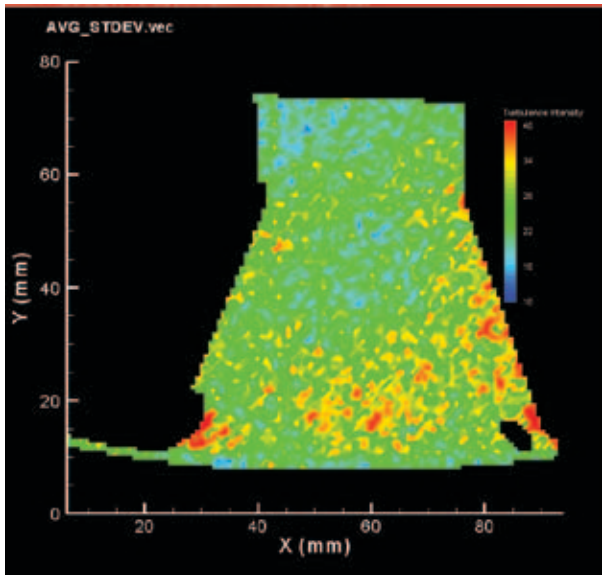

Figure 25

Turbulence Intensity Between Racks

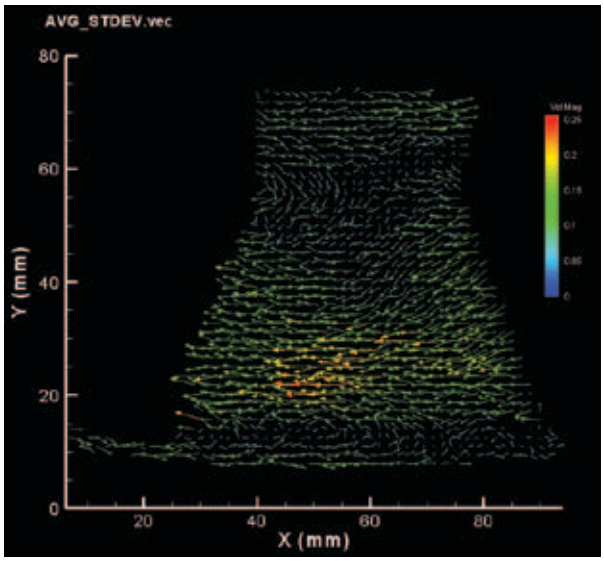

Figure 23

Velocity Flow Field Between Racks

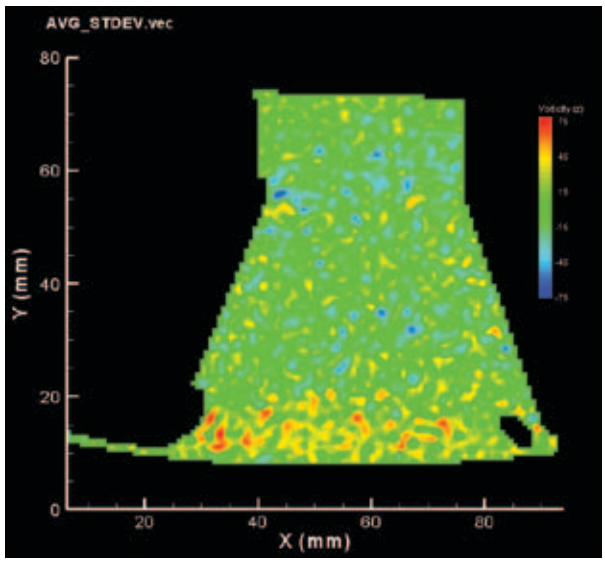

Figure 26

Vorticity Between Racks

PLIF Results for Tidal Agitation Processor

PLIF data was collected for a single cassette in both the upper and lower racks in the tidal agitation processor. The same modified cassette that was used in RTP processor was used here, except that the cassette was placed upside down to allow for the laser light to pass through the cassette from the top. Data for the lower rack was collected with the upper rack removed. This was done to allow the laser plane to reach the lower rack.

PLIF image for each rack are presented in Figures 27 and 28. In Figure 27, the visualized cassette is in the lower rack and for Figure 28, the cassette is in the upper rack. These images show the general flow field for a cassette located in each rack. It can be seen that in general the flow enters in the upper left and travels to the lower right. In addition, due to the wedge shape of the neighboring cassette to the right, fluid is diverted into the cassette from the right top side and exits the cassettes shortly after by the dominant flow from the top left corner. The magnitude of the velocity vectors in the cassettes of the lower rack are almost twice of those in the upper racks as shown by the PIV vectors of Figures 29, and 30. This is because the stirrer generates a low pressure region just below the first rack. Thus, the higher pressure gradient between the top and bottom surfaces of the lower rack compared with the upper rack creates larger flow speeds in the lower rack cassettes. It should be noted that the flow field in the lower rack does not reflect the presence of the upper rack. As such, the actual flow field with the upper rack present may differ slightly from the data collected.

The shedded vortices behind the cassette slots clearly observed in Figures 27 and 28 are similar to the ones observed for the RTP processor. However, the difference is that these vortices are distorted somewhat toward the bottom of the cassettes.

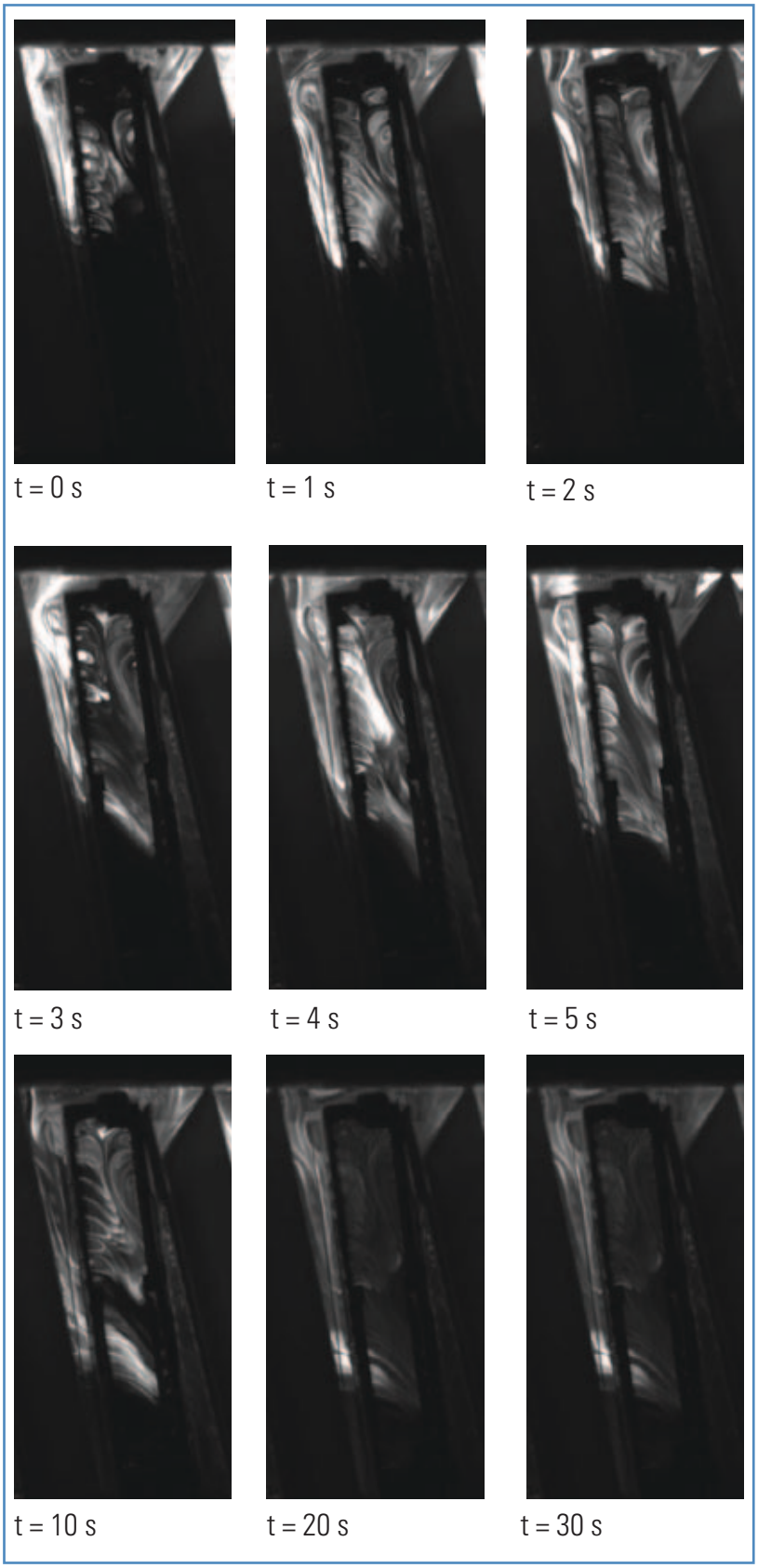

Figure 27

Visualized Flow in the Lower Rack Cassette

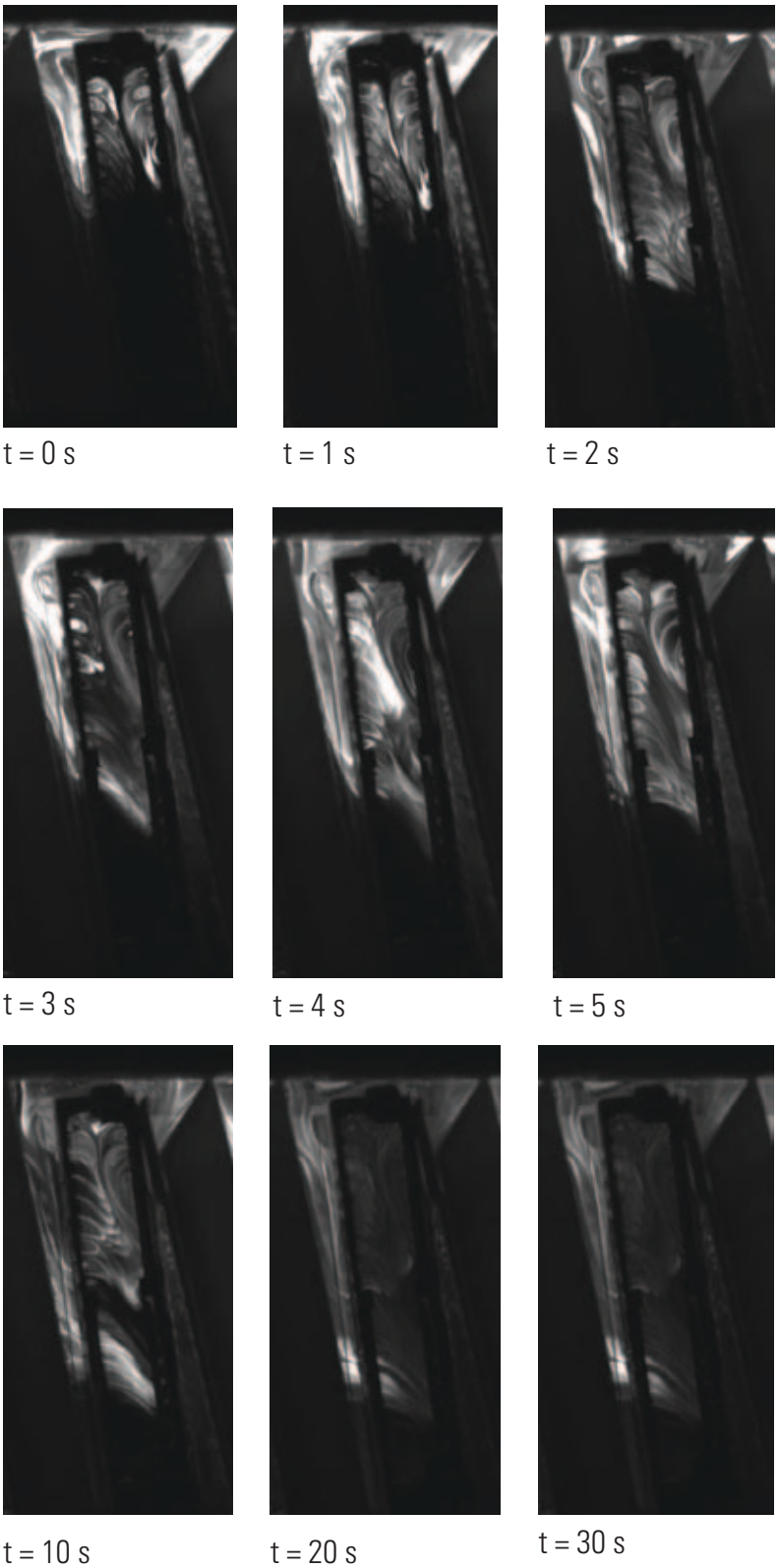

Figure 28

Visualized Flow in the Upper Rack Cassette

PIV Results for Tidal Agitation Processor

PIV data was collected for a single cassette located in both the upper and lower racks of the tidal agitation processor. Once again data for the lower rack was collected with the upper rack removed. A series of 20 images was collected for each rack and then averaged to obtain the characteristic flow field within the cassette of interest. Velocity flow fields, steam traces, turbulence maps, and vorticity maps were created for cassettes in each rack. These are presented in Figures 29-36.

It should be noted that velocity, turbulence, and vorticity in the lower rack are almost twice the values of the upper rack. This would be expected, since the lower rack is exposed directly to mixing flow generated by the stirrer. The presence of the upper rack would increase the amount of obstructions in the processor, and would be expected to impede the flow through any single cassette in the lower rack. As such, data collected for the lower cassette should not be used as an accurate reflection of actual flow conditions within the cassettes. However, it could be implied that the data for the upper rack most likely represents a similar flow field to the actual flow field in the lower rack when the upper rack is present.

The major difference between the mean velocity fields between the two processors, are the magnitudes and direction of the velocity vectors. The overall magnitude of the velocity vectors are approximately one order of magnitude smaller in the tidal agitation processor compared with the RTP processor. In addition, the tidal agitation processor fluid direction is along the cassette length, rather than being perpendicular to it like the RTP processor. Both of these differences would help to reduce the processing time in the RTP model.

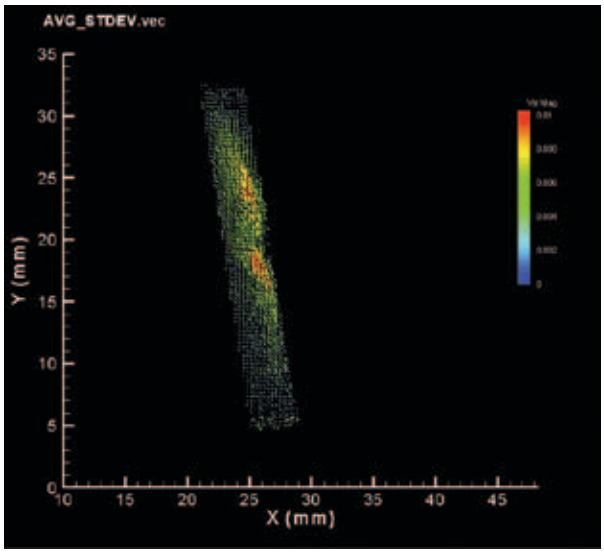

Figure 29

Velocity Flow Field, Lower Rack

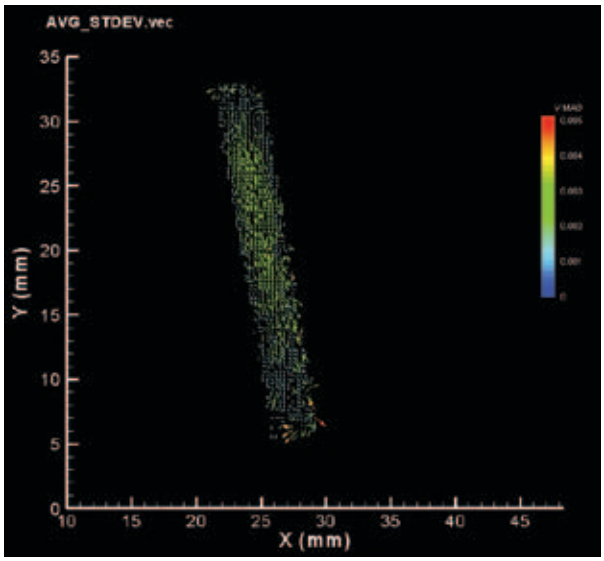

Figure 30

Velocity Flow Field, Upper Rack

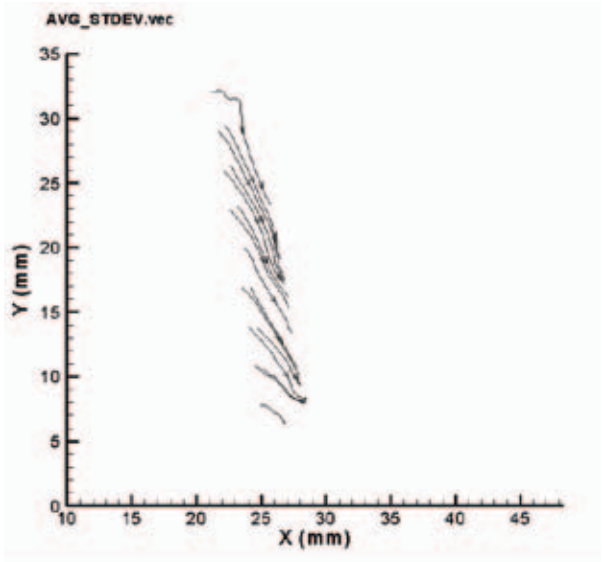

Figure 31

Stream Trace, Lower Rack

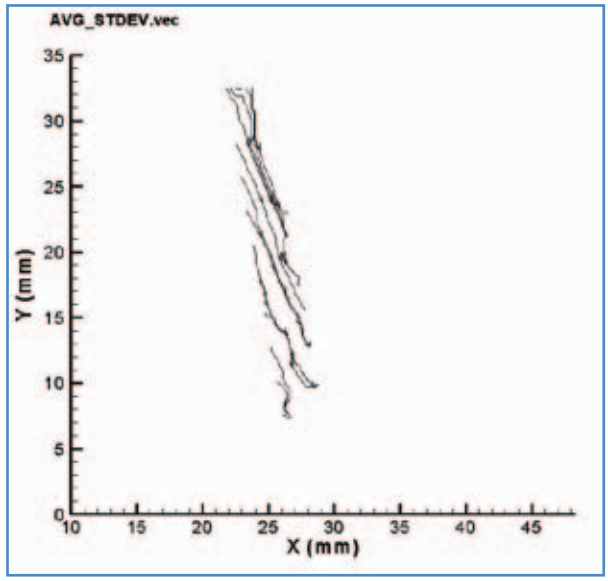

Figure 32

Stream Trace, Upper Rack

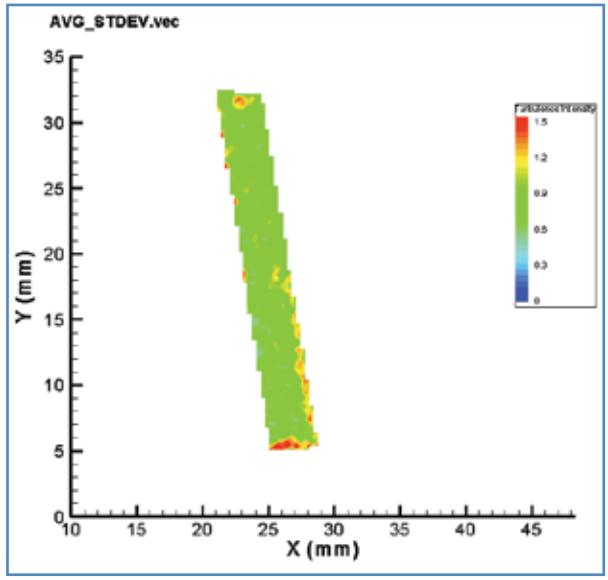

Figure 33

Turbulence Intensity, Lower Rack

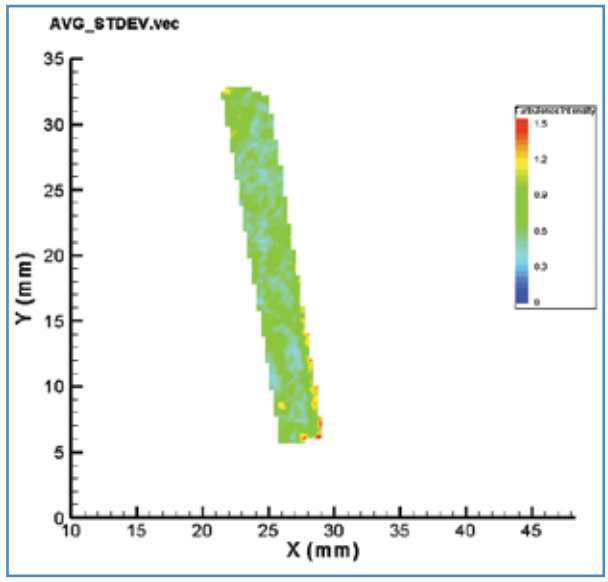

Figure 34

Turbulence Intensity, Upper Rack

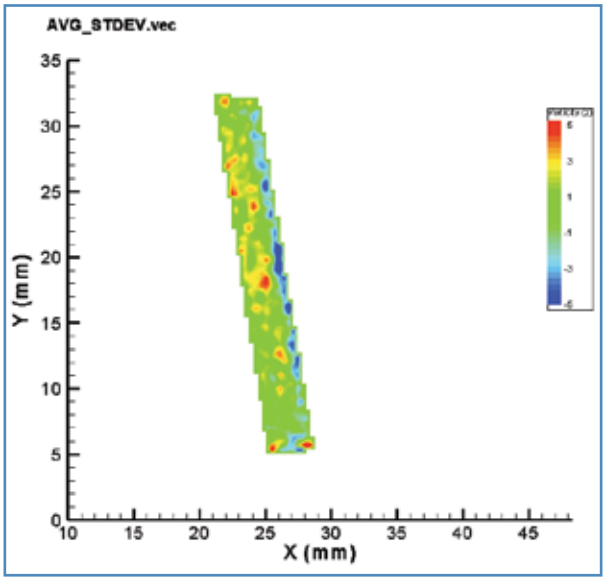

Figure 35

Vorticity, Lower Rack

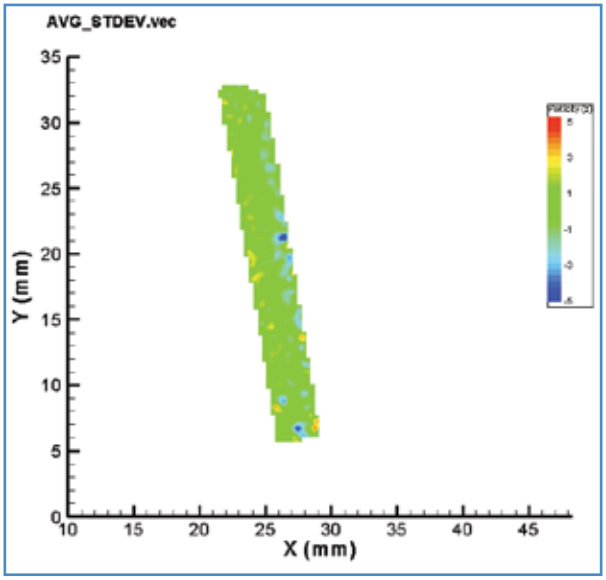

Figure 36

Vorticity, Upper Rack

Volume Flow Rate Calculations	
RTP Machine	**Tidal Agitation Machine**
Drainage Flow Rate Cassette Volume = 3721 mm^3 Drainage Cycles = 8 cycle/min Volume Flow Rate = 496 mm^3/sec	Drainage Flow Rate Cassette Volume = 3721 mm^3 Drainage Cycles = 0.05 cycle/min Volume Flow Rate = 3 mm^3/sec
Velocity Flow Rate Cassette Area = 709 mm^2 Average Flow Velocity = 65 mm/s Immersion Time = 40%/cycle Volume Flow Rate = 18434 mm^3/sec	Velocity Flow Rate Cassette Area = 709 mm^2 Average Flow Velocity = 4 mm/s Immersion Time = 100 %/cycle Volume Flow Rate = 2836 mm^3/sec
Total Volume Flow Rate = 18930 mm^3/sec	Total Volume Flow Rate = 2839 mm^3/sec

Table 2

Comparison of Results

It can be seen quantitatively from the PIV data for both machines that the mixing and velocities for the RTP processor are superior to the tidal agitation processor. However, it would be beneficial to quantify the extent of this superiority with a single number. As such, the overall volume flow through a single cassette could be used to achieve this.

The overall volume flow is defined as the amount of fluid that passes through a cassette per unit time interval. In this case we will perform calculations of volume flow in mm3/sec. Two processes determine the overall volume flow rate. Each cassette has an average fluid velocity passing through it when submerged, as well as fluid exchange due to drainage and filling. The overall volume flow is a summation of the two processes. In the case of the RTP processor the cassette drains and fills 8 times per minute, in line with the 8 rpm rotation speed. The tidal agitation processor drains and fills once every 20 minutes due to fluid exchange within the processor.

The volumetric flow rate due to fluid passing through the cassette will be referred to as submerged flow rate, and is calculated by multiplying the average fluid velocity through the cassette by the cross sectional area of the cassette. For the RTP case the submerged flow rate has to be further modified by the amount of time that the cassette is actually submerged for each rotation. This is referred to as immersion time. The volume flow due to drainage and filling of the cassette will be referred to as the drainage flow rate, and is calculated using the volume of the cassette and the number of drainage cycles per second. Average velocities were obtained from PIV measurements. The calculations of volume flow rate for both machines are shown in Table 2.

It can be seen from the calculations in Table 2, that volume flow rate in the RTP processor is far superior to the tidal agitation processor, and is almost 7 times larger. We could then imply that the RTP processor is 7 times as efficient as the tidal agitation processor machine.

PLIF Results for the Total Biopsy Cassette II

The PLIF images shown in Figure 37 show the details of the flow behavior for the Total Biopsy Cassette II, re-designed in the first phase of this research. The shedded vortices behind the five front holes inside the cassette, and the exit flow out f the 1 millimeter diameter holes in the back of the cassette as marked with the circles are observed in these photographs.

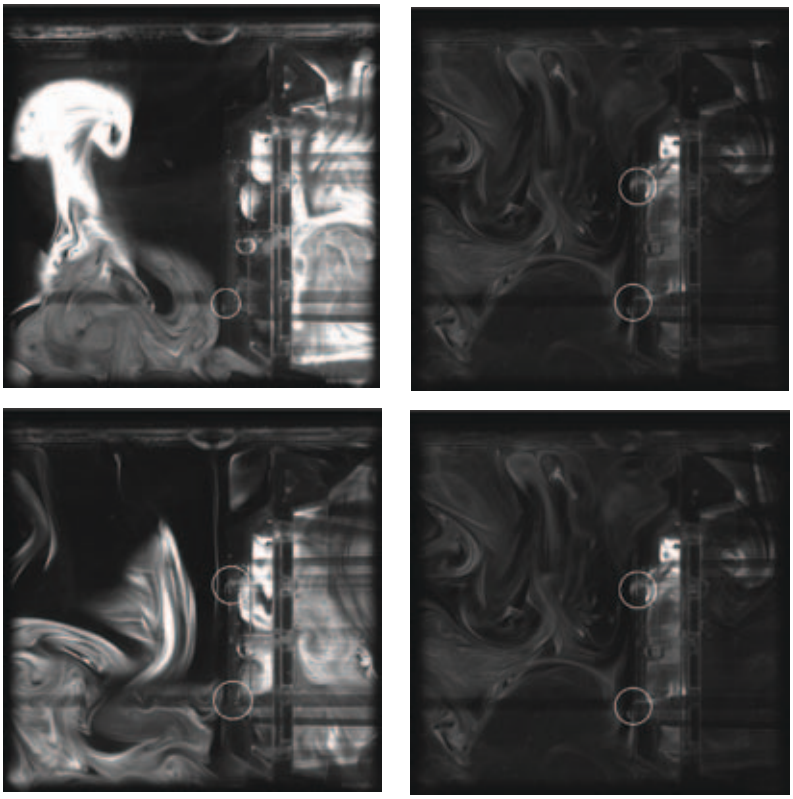

Figure 37

PLIF Images for the Total Biopsy Cassette II

Conclusions

The RTP processor is superior in all ways to the tidal agitation processor. The best measure of this is by comparison of the volume flow rates for the two machines as calculated in Table 2. This would indicate that the RTP processor is 7 times more efficient than the tidal agitation processor at passing fluid over the tissue samples.

Beyond the volume flow rate comparison, efficiency of the machines could be quantified by the amount of mixing occurring within the cassettes and in the processor as a whole. Turbulence and vorticity could be used as a rough measure of the amount of mixing occurring within the cassettes. It can be seen in the turbulence and vorticity maps that the magnitudes of these quantities are much larger in the RTP processor than the tidal agitation processor, and are on the order of 5 times larger in the RTP processor. Additionally, the researchers found the RTP cassette racks to be much easier to load and unload. This would seem to be an additional unquantifiable benefit of the RTP processor.

Further Discussion

There are several areas that were encountered while conducting the current research that could be more fully investigated. Some of these areas could have direct impact on the further development of the RTP processor, or refining the use of the processor.

Data was collected only for cassettes located near the center of the rack in the three outermost rows. It was assumed that these areas would be of greatest interest, and would be most representative of the flow within all cassettes. However, further research could be conducted to investigate the flow fields within cassettes located elsewhere in the racks. This information could be useful for determining optimal locations for larger tissue samples. It would be assumed that the flow fields would be superior in cassettes located closer to the edge of the rack at the inflow side. As such, larger tissue samples should be located there. However, the current research does not address this issue.

All data was collected for empty cassettes. This was to introduce a level of similarity between all sets of data being taken. The intent of the research was to compare the efficacy of the two processors, not to investigate effects of sample placement and size on the flow fields. Also, PIV measurements require a clear flow field, which would be impeded by the presence of a simulated tissue sample. However, it would be of some interest to determine the effects of tissue samples on the flow fields within the cassettes. This could be accomplished by placing tissue samples in the cassettes upstream of the cassettes of interest and then looking at the effect on the flow fields. The size and placement of the tissue samples could be varied to determine optimal loading of the tissue samples within the rack.

As stated in the conclusions, data was only taken when the racks were in the center of the fluid. Further research could be conducted to investigate the flow fields within the cassettes when they are entering and leaving the fluid.

Richard-Allan Scientific
Subsidiary of Thermo Fisher Scientific
4481 Campus Drive,
Kalamazoo, MI 49008
Phone: 1 (800) 522-7270
Phone: + 1 (269) 544-5600

Thermo Shandon Limited
Subsidiary of Thermo Fisher Scientific
Tudor Road, Manor Park,
Runcorn, Cheshire
WA7 1TA, UK
Phone: +44 (0) 1928 534 050
Fax: + 44 (0) 1928 534 049

www.thermoscientific.com/patholgy